Measurement of the diffusivity of fullerenes in polymers using bilayer organic field effect transistors

John G. Labram,[1] James Kirkpatrick,[2] Donal D. C. Bradley,[1] and Thomas D. Anthopoulos[1,*]
[1]*Department of Physics and Centre for Plastic Electronics, Blackett Laboratory, Imperial College London, London SW7 2BW, United Kingdom*
[2]*Mathematical Institute, 24-29 St Giles', University of Oxford, Oxford OX1 3LB, United Kingdom*
(Received 8 May 2011; published 18 August 2011)

Bilayer poly(3-hexylthiophene):[6,6]-phenyl C_{61}-butyric acid methyl ester ($PC_{61}BM$) [P3HT:$PC_{61}BM$] organic field-effect transistors (OFETs) have been fabricated using a bottom-contact, bottom-gate (BCBG) architecture. By annealing these devices and monitoring the magnitude of the electron field-effect mobility, information about the diffusion properties of $PC_{61}BM$ in P3HT can be obtained. Using a solution to the one-dimensional diffusion equation and an application of percolation theory, a relationship between electron field-effect mobility, diffusion coefficient, and annealing time has been obtained. By applying this model to time-dependent mobility measurements, a rough approximation of 5 nm^2s^{-1} has been made for the diffusion coefficient of $PC_{61}BM$ in P3HT at a temperature of 130 °C.

DOI: 10.1103/PhysRevB.84.075344 PACS number(s): 73.61.Ph, 73.61.Wp

I. INTRODUCTION

Because of their potential low cost, mechanical flexibility, and ease of production, the development of organic photovoltaic (OPV) solar cells is currently of huge scientific and commercial interest.[1,2] The organic solar cells with the highest reported power conversion efficiency (PCE) to date are generally based on a bulk heterojunction (BHJ) donor-acceptor structure, consisting of interpenetrating polymer and fullerene networks.[3,4] This structure is known to give rise to an extremely large interfacial area when compared to alternative systems,[5] resulting in increased exciton-dissociation efficiencies and hence PCEs. The internal microstructure of this system is of critical importance to the carrier-transport and exciton-dissociation efficiency of OPVs and is hence the subject of an intense research effort.[6–9] Unfortunately, however, because of their inherent structural complexity the microstructure of BHJs has so-far proven notoriously difficult to understand in any great detail.

Recently, equivalent bilayer structures have allowed for interesting insights into polymer:fullerene systems.[10–16] Using deposition techniques such as stamp transfer[10,12,15] and orthogonal solvents,[11,14,16] several groups have now reported bilayer structures based upon the well-studied system of poly(3-hexylthiophene) (P3HT) and [6,6]-phenyl C_{61}-butyric acid methyl ester ($PC_{61}BM$). Using techniques such as dynamic secondary ion mass spectrometry (DSIMS),[13,15] neutron reflectometry,[14] and transmission electron microscopy,[16] it has been observed that $PC_{61}BM$ will diffuse into P3HT upon annealing. This is a phenomenon distinct from the widely reported polymer-crystallization and fullerene-clustering process generally associated with improvements in OPV power-conversion efficiency.[17–19] Until recently this process was largely unknown and hence absent from any OPV processing and optimization procedures. In their study Treat *et al*. showed that the diffusion of $PC_{61}BM$ into P3HT takes place at relatively low temperatures (e.g., 50 °C) and over very short time scales (e.g., 30 s).[15] Using two-dimensional (2D) x-ray scattering in grazing incidence geometry (GIWAXS) they also showed that this diffusion takes place without any significant disruption to the crystalline P3HT domains in the film.

So far little has been said about the physical mechanism by which the diffusion of $PC_{61}BM$ into P3HT takes place in such structures. By gaining a solid understanding of this process, one could be given much greater control over desired OPV structures for potential device applications. With an accurate model describing the process, a calculation of relevant concentration profiles could be carried out and hence the composition profile of such OPVs could in the future be "tailor-made."

In this report we have used bilayer organic field-effect transistors (OFETs) to further study this diffusion phenomenon. OFET measurements have previously been shown to be capable of probing time- and temperature-dependent changes in the microstructure of polymer:fullerene blends with excellent sensitivity.[20,21] The three terminal structures of OFETs allows the selective injection of holes into the polymer network and/or electrons into the fullerene network, but not *vice versa*.[22,23] By monitoring the evolution of hole and electron field-effect mobilities in polymer:fullerene systems, changes in the percolation properties of these two networks at the semiconductor-dielectric interface can hence be inferred.

Using a P3HT:$PC_{61}BM$ bilayer OFET combined with a bottom-contact, bottom-gate (BCBG) architecture, we have here measured the diffusion of $PC_{61}BM$ in P3HT indirectly via field-effect mobility measurements. In order to convert the field-effect transistor (FET) mobility to $PC_{61}BM$ concentration we propose an elegant model based on percolation theory. The main advantage of this model is that the functional dependence of mobility on concentration depends on two parameters only: a scaling parameter for the mobility and one for distance. We then employ a simple one-dimensional ordinary-diffusion model to fit the resulting time-dependent measurement and hence estimate the diffusion coefficient of $PC_{61}BM$ in P3HT. The model presented within this paper is the first attempt to quantitatively describe this diffusion process and hence provide guidelines for future device processing and optimization procedures.

II. EXPERIMENTAL METHODS

Bilayer BCBG transistors were fabricated on highly doped (n^{++}) silicon wafers, which acted as the gate electrode, with a 200-nm thermally grown silicon dioxide layer as the gate dielectric. The silicon dioxide surfaces were then passivated with hexamethyldisilazane. Gold source and drain electrodes were defined using standard photolithographic techniques. Solutions of P3HT were then deposited onto the substrates via spin coating. The solvent used was chlorobenzene. $PC_{61}BM$ was deposited onto the P3HT via thermal sublimation under high vacuum (10^{-9} bar) at an average rate of 0.3 $Å s^{-1}$. The $PC_{61}BM$ started to sublime at a temperature of 220 °C, approximately 200 °C lower than for C_{60}.

Since $PC_{61}BM$ has never, to the knowledge of the authors, been reported to have been deposited via thermal sublimation, it is important to ensure that the $PC_{61}BM$ has indeed been deposited as expected, without degradation attributable to heating. The normalized optical absorption spectra of vacuum-deposited $PC_{61}BM$, spin-cast $PC_{61}BM$, and vacuum-deposited C_{60} are hence shown in Fig. 1(a). These films were deposited onto quartz and measured with a Shimadzu UV-2550 ultraviolet-visible spectrophotometer. Top-contact, bottom-gate (TCBG) pristine $PC_{61}BM$ OFETs were also fabricated on highly doped silicon and silicon dioxide. The silicon dioxide layer was in this case passivated with a thin (~50 nm) layer of divinyltetramethyldisiloxane-bis(benzocyclobutene) (BCB). $PC_{61}BM$ was deposited onto the BCB-coated Si/SiO_2 substrates via thermal sublimation and spin coating. 50-nm aluminum source and drain electrodes were then deposited via thermal evaporation under high vacuum through shadow masks at an average rate of 1 $Å s^{-1}$. The transfer characteristics of 10 vacuum-deposited and 10 spin-cast TCBG $PC_{61}BM$ OFETs were measured under N_2 without annealing. Example transfer characteristics of (b) vacuum-deposited and (c) spin-cast $PC_{61}BM$ OFETs are shown in Fig. 1. A schematic representation of this OFET structure is given in the inset of Fig. 1(c).

The data in Fig. 1 provides strong evidence that the material being deposited via thermal sublimation is indeed $PC_{61}BM$, as opposed to (say) C_{60} formed from $PC_{61}BM$ that underwent degradation during the evaporation process. The average electron field-effect mobility was measured to be $3 \pm 2 \times 10^{-2}$ $cm^2V^{-1}s^{-1}$ for the vacuum-deposited $PC_{61}BM$ OFETs and $8.1 \pm 0.7 \times 10^{-2}$ $cm^2V^{-1}s^{-1}$ for the spin-cast $PC_{61}BM$ OFETs. These values are comparable with previous reports of $PC_{61}BM$ OFETs on BCB substrates[24] and are significantly lower than similar devices with C_{60} as the active layer.[25] The difference in the average and standard deviation of the mobilities is attributed to differences in the film microstructure, caused by the different deposition methods. Similarly, the higher threshold voltage observed for vacuum-deposited $PC_{61}BM$ [see Fig. 1(b)] with respect to spin-cast $PC_{61}BM$ [see Fig. 1(c)] is attributed to differences in the microstructure at the semiconductor-electrode interfaces.

The bilayer structure employed in this study is shown in Fig. 2(a). P3HT (95% regioregularity; weight-average molecular weight, $M_w \sim 60$ kg/mol) was obtained from Merck Chemicals. $PC_{61}BM$ was obtained from Solenne B.V. and was >99.5% pure. The chemical structures of P3HT and $PC_{61}BM$ are shown in Fig. 2(a). Transistor fabrication and electrical characterization was carried out under ambient pressure in N_2 without exposure in air using a Keithley 4200 semiconductor parameter analyzer. The mobilities of charge carriers were estimated in the saturation regime using standard semiconductor models:[26]

$$\mu = \left(\frac{\partial\sqrt{I_D}}{\partial V_G}\right)^2 \frac{2L}{WC_i}. \quad (1)$$

Here I_D is the measured drain current in the saturation regime, V_G is the applied gate voltage, L and W are the OFET channel length and width, respectively, and C_i is the geometrical capacitance of the gate dielectric. The film thicknesses were measured using an Agilent 5500 atomic force microscope in tapping mode.

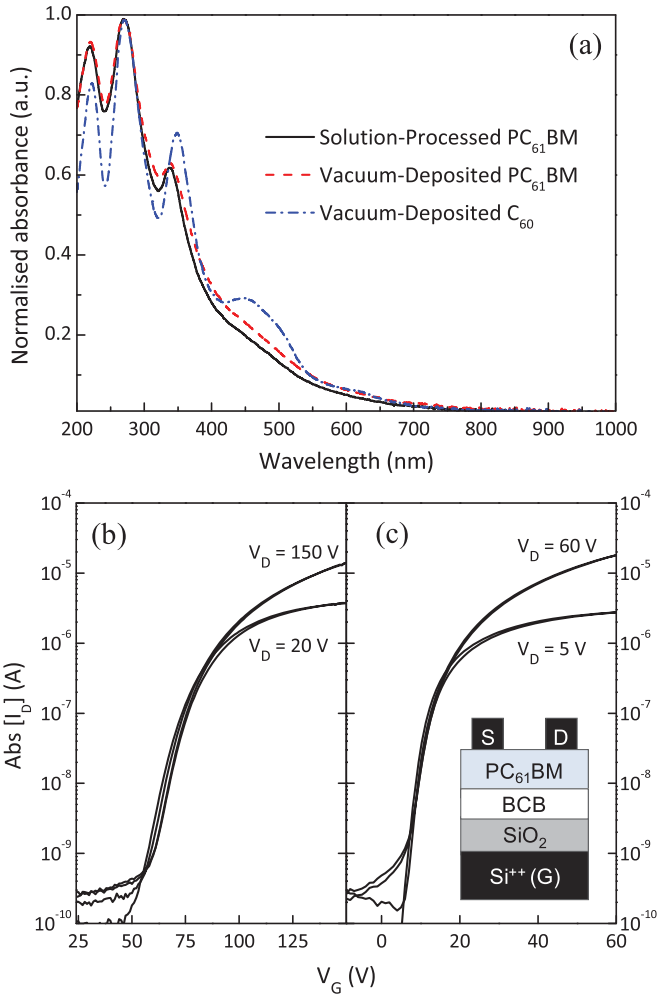

FIG. 1. (Color online) (a) Normalized optical-absorption spectra of spin-cast $PC_{61}BM$, vacuum-deposited $PC_{61}BM$, and vacuum-deposited C_{60}. Transfer characteristics of (b) spin-cast $PC_{61}BM$ and (c) vacuum-deposited $PC_{61}BM$ TCBG OFETs fabricated on BCB-coated SiO_2 with aluminium source and drain electrodes. The devices were characterized under ambient pressure in N_2 without being annealed. In both cases the transistors had channel lengths and widths of 40 μm and 1000 μm, respectively. Inset to (c): schematic diagram of TCBG transistor structure employed.

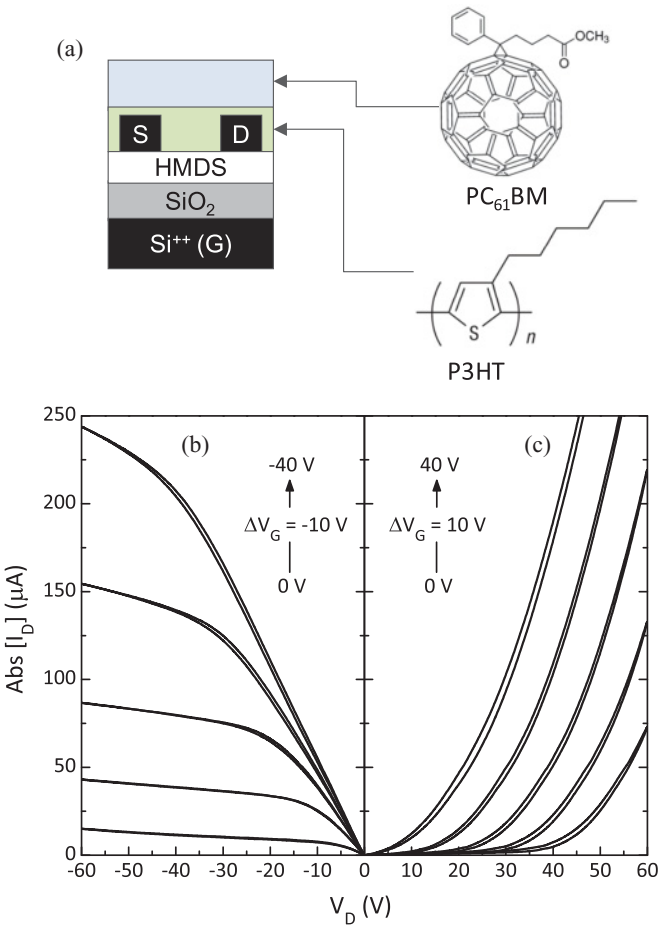

FIG. 2. (Color online) (a) Schematic diagram of BCBG bilayer OFET structure used in this study and molecular structures of $PC_{61}BM$ (top) and P3HT (bottom). Output characteristics of example bilayer P3HT:$PC_{61}BM$ BCBG transistors measured under ambient-pressure N_2 before annealing with applied gate voltages of (b) $V_G = 0$ V to $V_G = -40$ V and (c) $V_G = 0$ V to $V_G = 40$ V. This device had a channel length and width of 7.5 μm and 10 000 μm, respectively, and P3HT and $PC_{61}BM$ thicknesses of 8 nm and 31 nm, respectively.

III. EXPERIMENTAL RESULTS

Example output characteristics of a P3HT:$PC_{61}BM$ bilayer OFET are shown in Fig. 2 with applied gate voltages between (b) $V_G = 0$ V and $V_G = -40$ V and (c) $V_G = 0$ V and $V_G = 40$ V. The thicknesses of the P3HT and $PC_{61}BM$ layers in this case were 8 nm and 31 nm, respectively. The observed characteristics are indicative of unipolar (p-type) behavior.[23] Since initially only P3HT is in contact with the source and drain electrodes and with the semiconductor-dielectric interface and because carrier transport only takes place within the first few nanometers from the semiconductor-dielectric interface,[27] this behavior is as expected. Bilayer ambipolar OFETs have previously been demonstrated for electronic[28] and light-sensing applications,[29] but in both these cases the architecture has been the so-called "middle-contact," where the source and drain electrodes have been in direct contact with both semiconductor systems. In such bilayer devices, the bottom semiconductor layer acts as the dielectric for the top semiconductor. Multilayer ambipolar systems have, however, previously been demonstrated using BCBG[30] and TCBG[31] architectures, where the electrodes have been in direct contact with one semiconductor only. This is in contrast to our system, where no n-channel is measurable initially. This difference in behavior is likely to be attributable to differences in the energy levels of the semiconductors and electrodes. Fully annealed (interdiffused) bilayer P3HT:$PC_{61}BM$ OFETs have recently been shown[16] to exhibit ambipolar behavior, as expected from a standard BHJ structure.[20,22] Given the data shown in Figs. 2(b) and 2(c) we can hence be confident that in our devices the measured mobility is representative of the state of the semiconductor system at the semiconductor-dielectric interface.

Several bilayer OFETs were annealed at temperatures between 60 °C and 300 °C in 20 °C steps, with each annealing step lasting 30 minutes. In this case the P3HT- and $PC_{61}BM$-layer thicknesses were 8 nm and 40 nm, respectively. The hole and electron mobilities of five OFETs were then measured in the saturation regime at room temperature after each annealing step. All annealing steps and measurements were carried out under N_2 without exposure to air. The average field-effect mobilities of these five devices are plotted as a function of annealing temperature in Fig. 3(a). Initially, no electron mobility is measurable in any device, and the average is therefore plotted as 10^{-9} $cm^2V^{-1}s^{-1}$, which is close to the measurement limits of our experimental setup.

Up to an annealing temperature of 100 °C the hole mobility remains constant and the electron mobility is undetectable. This is likely to be because the extent of $PC_{61}BM$ diffusion has not been sufficient for a strong percolation network to form at the semiconductor-dielectric interface. Although some diffusion is expected to take place at temperatures as low as 50 °C, the $PC_{61}BM$ miscibility in P3HT is known[15] to be temperature dependent. Since the $PC_{61}BM$ layer is five times as thick as the P3HT layer, it is therefore anticipated that there will be a strong dependence of electron mobility on annealing temperature.

After annealing to 120 °C and 140 °C the electron mobility becomes measurable. This is believed to be because of $PC_{61}BM$ having diffused from the top layer of the device through the P3HT to the semiconductor-dielectric interface. Between 80 °C and 140 °C the hole mobility falls by a factor of five. This is attributed to the presence of diffused $PC_{61}BM$ disrupting the P3HT packing at the bottom interface. Although the presence of diffused $PC_{61}BM$ is known not to disrupt the crystalline P3HT domains in thick (∼100 nm) films,[15] here we have an 8-nm-thin film and the two systems are therefore not likely to be directly comparable. The fact that at 100 °C the hole mobility falls, while the electron mobility remains unmeasurable is likely to be attributable to the insufficient concentration of $PC_{61}BM$ at the bottom interface.

At an annealing temperature of 160 °C, the electron mobility falls to a value of $\sim 10^{-6}$ $cm^2V^{-1}s^{-1}$. This is attributed to the thermally induced P3HT-crystallization and $PC_{61}BM$-clustering process that has previously been associated with improvements in OPV performance.[17,18] This process is believed to lead to a reduction in the concentration of $PC_{61}BM$ in regions between clusters,[32] and therefore a

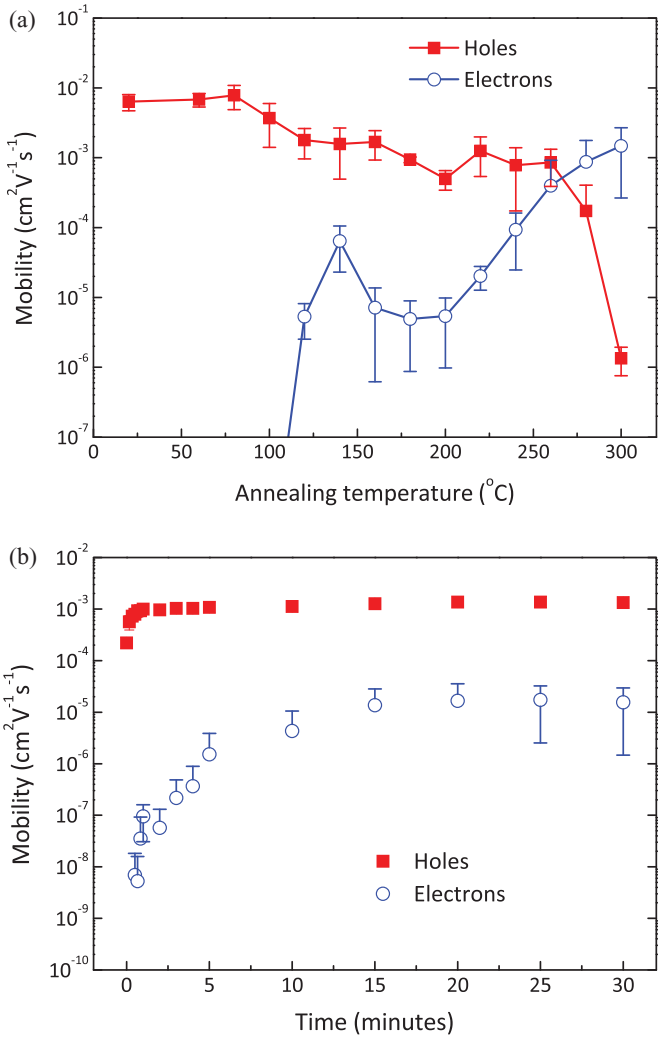

FIG. 3. (Color online) (a) Average saturation-regime field-effect mobility of holes and electrons in five bilayer P3HT:PC_{61}BM OFETs measured at room temperature under ambient-pressure N_2 after being annealed at various temperatures for 30 minutes. The error bars represent the standard deviation in the measured field-effect mobility. When the electron mobility was not detectable it was plotted as 10^{-9} $cm^2V^{-1}s^{-1}$. The thicknesses of the P3HT and PC_{61}BM layers were 8 nm and 40 nm, respectively. (b) Average saturation-regime field-effect mobility of holes and electrons in five bilayer P3HT:PC_{61}BM transistors measured under ambient-pressure N_2 after being annealed at 130 °C, plotted as a function of time. The thicknesses of the P3HT and PC_{61}BM layers were in this case 25 nm and 31 nm, respectively.

reduction in electron percolation-pathways, causing a measurable reduction in electron field-effect mobility.[20,21] While clearly detrimental to the field-effect mobility, the same process in different structures is known to result in an increase in electron mobility.[19] This difference is explainable when considering the significant differences in device architecture and hence electron percolation-pathways.[20]

At temperatures of 220 °C and above the electron mobility is observed to rise, and the hole mobility begins to fall. This is because of the melting of the P3HT:PC_{61}BM blend and subsequent cooling into an amorphous state.[20,33]

Figure 3(b) shows the average hole and electron mobilities of five bilayer P3HT:PC_{61}BM OFETs (P3HT and PC_{61}BM thicknesses: 25 nm and 31 nm, respectively) measured at room temperature after various periods of annealing at 130 °C. In this case the hole mobility is observed to rise by a factor of four in the first 60 seconds of annealing and then saturate at a constant value. This is possibly because of enhanced charge-transport pathways caused by P3HT crystallization. The fact that the hole mobility does not fall as PC_{61}BM diffuses through it is consistent with previous reports of the P3HT crystalline domains not being disrupted by the presence of PC_{61}BM.[15] The apparent discrepancy with the data in Fig. 3(a), where the hole mobility falls as PC_{61}BM diffuses through the P3HT, is attributed to differences in P3HT thickness and hence different crystalline domain sizes.

The electron mobility is not measurable for the first 20 seconds of annealing, after which it rises quickly before slowly saturating to a constant value. This is believed to be attributable to fullerenes diffusing from the PC_{61}BM layer into the P3HT and finally reaching a homogeneous distribution. The time-scale of this process is markedly different than observed in the study by Treat *et al.*, where the diffusion process was observed to be complete after just 30 s of annealing.[15] It is likely that factors such as the difference in annealing temperature (150 °C compared to 130 °C here) or possible differences in P3HT molecular weight and regioregularity,[34] may be the cause of this discrepancy. It is also possible that, once percolation has been reached, FET mobility measurements will reveal changes in concentration that may not be detectable via alternative techniques. The mobility of charge carriers in a FET device are known to be exponentially dependent on the hopping distance between states.[35] Hence even very small changes in the PC_{61}BM concentration at the semiconductor-dielectric interface are expected to lead to significant changes in the measured field-effect mobility. It should be noted however that FET measurements are limited by the onset of percolation, before which the sensitivity of the technique is inadequate for the statements about the fullerene concentration to be made.

Despite the observed discrepancy with previous results, the data presented in Fig. 3(b) suggests that, given this structure and the material parameters employed here, the diffusion of PC_{61}BM in P3HT takes place with a time scale of minutes. Example transfer characteristics for various periods of annealing are given in supporting information Fig. S1.

IV. MODELING THE EVOLUTION OF ELECTRON MOBILITY

The time dependence of electron mobility with annealing time, as exhibited in Fig. 3(b), should allow a rough estimate of the diffusion coefficient for this process to be made. In this section a simple model based upon Fick's 2nd law (i.e., the diffusion equation) and percolation theory is derived, relating the electron field-effect mobility to the annealing time and the diffusion coefficient of PC_{61}BM in P3HT. Given the simplicity of the bilayer system, we can consider diffusion in only one dimension. It should be noted that the purpose of this section is to extract an approximate value for the diffusivity of PC_{61}BM

in P3HT, not provide a rigorous theoretical description of the diffusion process.

The diffusion equation in one dimension is given in the following,

$$\frac{\partial C(x,t)}{\partial t} = D\frac{\partial^2 C(x,t)}{\partial x^2}. \tag{2}$$

Here $C(x,t)$ is the 2D $PC_{61}BM$ concentration at a distance x from the semiconductor-dielectric interface a time t after diffusion (annealing) has begun. By considering the structure of the OFET in Fig. 2(a), the initial distribution of $PC_{61}BM$ can be expressed as

$$C(x,0) = \begin{cases} 0 & \text{for } 0 \leqslant x \leqslant x_p \\ C_0 & \text{for } x_p \leqslant x \leqslant x_c \end{cases}. \tag{3}$$

Here C_0 is the 2D $PC_{61}BM$ concentration in the pristine $PC_{61}BM$ layer, x_p is the distance of the P3HT:$PC_{61}BM$ interface from the dielectric-semiconductor interface (i.e., the P3HT thickness), and x_c is the distance of the top of the $PC_{61}BM$ layer from the dielectric-semiconductor interface (i.e., the P3HT thickness + the $PC_{61}BM$ thickness). It is assumed that all interfaces are perfectly flat.

We assume that both the semiconductor-dielectric and the top $PC_{61}BM$ interfaces allow no material flow across them. This assumption then leads to the following two boundary conditions:

$$\frac{\partial C(0,t)}{\partial x} = 0 \tag{4}$$

$$\frac{\partial C(x_c,t)}{\partial x} = 0. \tag{5}$$

Given the initial distribution (3) and the boundary conditions (4) and (5), the diffusion Eq. (2) can be solved using standard techniques[36] to give

$$C(x,t) = C_0\left(1 - \frac{x_p}{x_c}\right) - C_0\sum_{n=1}^{\infty}\frac{2}{n\pi}\sin\left(\frac{n\pi x_p}{x_c}\right) \times \exp\left(-\frac{n^2\pi^2 Dt}{x_c^2}\right)\cos\left(\frac{n\pi x}{x_c}\right). \tag{6}$$

This equation has been evaluated and plotted as a function of x for various times in Fig. 4(a). As $t \to \infty$ the concentration becomes homogeneous throughout the device with a value of C/C_0 equal to $(x_c - x_p)/x_c$, i.e., the thickness of the $PC_{61}BM$ layer divided by the thickness of both layers combined.

Since charge transport in OFETs is known[27] to only take place within the first few nanometers from the semiconductor-dielectric interface, we can consider the concentration at $x = 0$ to be representative of that measured using our devices. That is,

$$C(0,t) = C_0\left(1 - \frac{x_p}{x_c}\right) - C_0\sum_{n=1}^{\infty}\frac{2}{n\pi}\sin\left(\frac{n\pi x_p}{x_c}\right) \times \exp\left(-\frac{n^2\pi^2 Dt}{x_c^2}\right). \tag{7}$$

Percolation theory on random-resistor networks can be applied to evaluate the electron mobility in terms of the $PC_{61}BM$ concentration.[37,38] This classic problem of critical phenomena

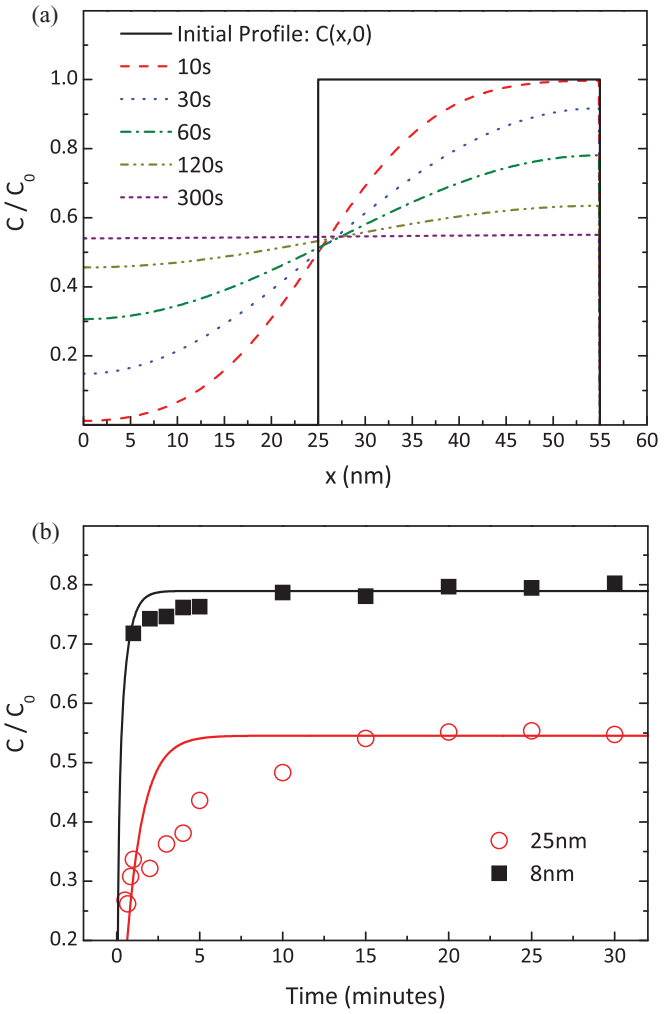

FIG. 4. (Color online) (a) Initial 2D concentration profile (C/C_0) of $PC_{61}BM$ in bilayer P3HT:$PC_{61}BM$ organic FET with P3HT and $PC_{61}BM$ thicknesses of 25 nm and 31 nm, respectively [Eq. (3)] and $PC_{61}BM$ concentration profile calculated using Eq. (6), evaluated at various times. The parameters used in this calculation were: $x_p = 25$ nm, $x_c = 55$ nm, and $D = 5$ nm^{2}s^{-1}. (b) Points: average $PC_{61}BM$ concentration calculated using Eq. (11) and saturation-regime field-effect mobility of electrons measured using two sets of bilayer P3HT:$PC_{61}BM$ transistors measured under ambient-pressure N_2 after being annealed at 130 °C, plotted as a function of time. The $PC_{61}BM$ thickness was 31 nm in both devices. The curves represent a best-fit to the experimental data using Eq. (7). The extracted diffusion coefficient in this case was found to be $D = 5$ nm^{2}s^{-1}.

is conceptualized as a typical example of a bond percolation problem. The key idea is that a critical concentration p_c exists below which percolation is exponentially unlikely (see Fig. 5). In such cases a network of nearest neighbors is extremely unlikely and the conductance of the network is effectively zero. At percolation and above it, conductance becomes possible. Computational studies show the conductance scales as

$$\overline{\sigma} = (p - p_c)^{1.43}, \tag{8}$$

where p is the bond percolation occupation and $\bar{\sigma}$ is proportional to the conductance. The percolation threshold p_c is well known for a square, 2D lattice and is $1/2$.[39] This suggests that,

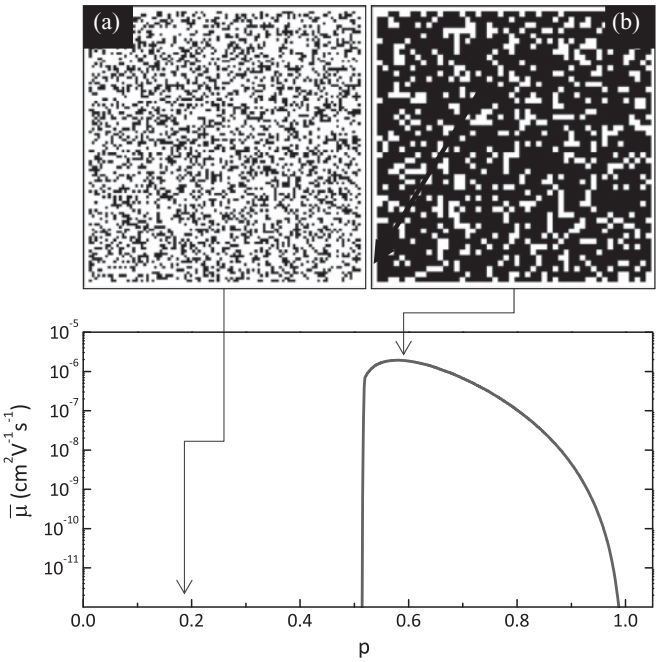

FIG. 5. Graphic illustrating how the electron field-effect mobility is computed for $\alpha = 0.1$, $\mu_0 = 1$, and $C/C_0 = 0.3$ using Eq. (11). The x axis shows the desired bond-occupation probability. On the y axis is mobility. As p is increased, the lattice constant necessary to obtain that particular p is also increased. Inset (a) shows a 100×100-random lattice with $c = 0.3$ and $a = 1$. This corresponds to a bond-occupation probability of 0.09 and hence a mobility of zero. Inset (b) shows the same lattice rescaled with $a = 2$. The lattice is now much better connected and the mobility is nonzero. Note the conductance is severely limited by the increase in lattice constant.

if $PC_{61}BM$ were capable of conducting charge only to their nearest neighbors, conductance would be possible only if the volume percentage of $PC_{61}BM$ exceeded $\sqrt{1/2} \approx 0.7$. Note that taking the square root is necessary because we are converting from site-occupation probabilities to bond-occupation probability. Clearly this is an overly pessimistic assumption: $PC_{61}BM$ are capable of conducting electrons to next nearest molecules, albeit at the cost of reduced conductance. Imagine that we now rescale our lattice, substituting 2×2-lattice points with one new super-lattice point. The points on the super lattice are considered occupied if any one of the previous lattice points was occupied. Thus, increasing the lattice constant of our lattice will massively increase the connectivity of our graph, bringing a system below percolation closer to percolation. However, it will also decrease the overall conductance as we expect that conductance between $PC_{61}BM$ falls exponentially with increasing distance. The balance of these two effects will give the conductance of the network. To express this concept mathematically, the first task is to determine the ratio of the new lattice constant to the original lattice constant a, which will lead to a certain bond occupation probability p given that the site occupation probability is c (i.e., $c = C/C_0$). Elementary probability considerations tell us that this is

$$a(p,c) = \sqrt{\frac{\log(1-\sqrt{p})}{\log(1-c)}} \quad \text{if } p,c < 1. \tag{9}$$

Notice that there is one trivial case for this equation: if the site occupation probability is 1, the bond occupation probability must be 1 at a lattice constant of 1.

Therefore, the conductivity of the $\bar{\sigma}$ can be written as

$$\bar{\sigma}(c) = \max\left[(p-p_c)^{1.43} e^{-\frac{\alpha(p,c)-1}{\alpha}}\right] \quad \text{with} \quad p > p_c, p > c^2, \tag{10}$$

where α is the natural length for decay of the conductance and the maximization is performed with respect to the bond-occupation probability p. Notice the two conditions that the bond occupation must satisfy: it must be greater than the percolation threshold, and it must be greater than c^2 to ensure that the lattice constant is always greater than 1. A maximum for the conductance is obtained when $c = 1$, in which case the conductance becomes $(1/2)^{1.43}$. With this in mind, and remembering that conductance and mobility are directly proportional, we model mobility as

$$\bar{\mu}(c) = \mu_0 2^{1.43}\left[\max(p-p_c)^{1.43} e^{-\frac{\alpha(p,c)-1}{\alpha}}\right] \quad \text{with} \quad p > p_c, p > c^2, \tag{11}$$

where μ_0 is the mobility of a pure $PC_{61}BM$ film. This model assumes that the conductance between two molecules depends only on the distance between them and not, for example, on energetic disorder. This assumption can be made because the purpose of this study is to understand how the electron mobility varies with 2D $PC_{61}BM$ concentration, not on other effects such as that of the gate field.[35] Furthermore we assume that the bond-percolation threshold is the same as for a square lattice, whereas the fullerene molecule's position is free to occupy any point in space, note, however, that the universal exponents will not be changed by changes in the lattice shape. A more significant assumption is that the position of fullerene molecules is random. This implies that there are no correlations in the position of the molecules, i.e., that there is no aggregation. Intuitively, we expect that aggregation would greatly increase the percolation threshold and—for a given concentration—diminish the effective mobility.[20]

One of the great powers of this approach is that the model has only two parameters: α and the scaling factor for the mobility. As is evident from Fig. 3(b), at long times (e.g., >15 minutes) the $PC_{61}BM$ diffuses to an even distribution equal to the average concentration as $t \to \infty$. Combined with similar data for a bilayer device with a P3HT thickness of 8 nm (data not shown), this allows us to extract the ratio of the mobility at two concentrations, which is independent of μ_0. The value of α that we obtain is 0.105. If we assume that the lattice constant is 1 nm (attributable to the approximate size of $PC_{61}BM$ molecules), this corresponds to a distance of 1.05 Å. If furthermore we assume that the conductance is proportional to the square of a tunneling matrix element, this would suggest the decay length for the matrix element is approximately 0.5 Å. It is now possible to fit μ_0 as 5.2×10^{-3} $cm^2V^{-1}s^{-1}$, which agrees well with previous experimental measurements of pristine $PC_{61}BM$ OFETs using a similar BCBG architecture.[20]

Knowing the relationship between concentration and mobility, we can convert the experimentally measured time-dependent electron mobility to a relationship between time

and concentration at the bottom of the film, allowing direct comparison with Eq. (7). The only free parameter is now the diffusivity D, which we fit to the data for the 25-nm polymer film and find to be 5 nm^2s^{-1}. This value of diffusivity seems reasonable given the length and time scales involved but is significantly lower than the value of $D = 3 \times 10^{-10}$ cm^2s^{-1} reported in the study by Treat *et al.*[15] As mentioned in Sec. III, it is believed that this difference can be explained by either differences in the material systems and/or annealing temperature, or possibly the extremely strong dependence of FET mobility measurements on fullerene concentration once percolation has been reached. While there are no observable changes in concentration profile after annealing at 150 °C for more than 30 seconds via DSIMS, it is expected the extreme relationship between mobility and concentration in Eq. (11) will result in further time-dependent information being revealed at times beyond that resolvable with DSIMS. Discrepancies between our evaluated value of D and that previously reported for the P3HT-crystalisation/$PC_{61}BM$-clustering process[32] can be ignored because it is a process distinct from that being studied here.

The diffusion coefficient computed for the thicker polymer film describes the thinner one reasonably well, however, the experimental concentration is observed to rise more quickly initially than the model suggests and then saturate more slowly. Our description of the relationship between mobility and concentration is based on the assumption that fullerenes are placed at random. This is equivalent to assuming that fullerenes do not interact with each other and aggregate. However this is unlikely to be true; $PC_{61}BM$ aggregation has previously been observed in P3HT:$PC_{61}BM$ blends with annealing temperatures as low as 130 °C.[40] This is likely to result in the concentration being underestimated for low values of t. Nonetheless, it is felt that this model serves as a good first attempt to quantify the diffusion process in this system and that the extracted value of diffusivity could serve to help future understanding and optimization of polymer:fullerene systems for OPV applications.

V. CONCLUSIONS

A study into the diffusion of $PC_{61}BM$ in P3HT has been carried out using bilayer OFETs. Because of the position of the semiconductor-dielectric interface and the source/drain electrodes relative to the semiconductor layers, the bilayer OFETs were observed to be initially hole-transporting only. Upon annealing these devices an electron channel is observed to form. This is attributed to the diffusion of $PC_{61}BM$ from the top layer through the P3HT to the semiconductor-dielectric interface (where charge transport in OFETs takes place) and subsequent formation of an electron-transporting percolation pathway. By measuring the evolution of the electron mobility as a function of annealing time, an insight into the time-dependence of this process is gained. Using a simple one-dimensional diffusion equation-based model and an application of percolation theory, a rough estimate of the diffusion coefficient of $PC_{61}BM$ in P3HT at an annealing temperature of 130 °C was found to be $D = 5$ nm^2s^{-1}. This study demonstrates that transistors can be a powerful tool in understanding the microstructural and charge-transport properties of polymer:fullerene blends for OPV applications. The proposed technique/approach can clearly be applied to other polymer:fullerene systems, potentially improving our understanding and the optimization procedures. The model presented here provides, albeit with some limitations, a first-step quantitative description of the diffusion process for fullerenes in polymers in such bilayer structures. This description, once built upon, could be used to allow much greater understanding and control of polymer:fullerene systems and lead to the development of more efficient OPV devices.

ACKNOWLEDGMENTS

This work was funded by the Engineering and Physical Sciences Research Council (EPSRC) grant number EP/F023200 and Research Councils UK (RCUK). TDA is an EPSRC Advanced Fellow and a RCUK Fellow/Lecturer. JK thanks the James Martin 21st Century School for funding. DDCB is the Lee-Lucas professor of Experimental Physics.

*thomas.anthopoulos@imperial.ac.uk

[1] C. J. Brabec, N. S. Sariciftci, and J. C. Hummelen, Adv. Funct. Mater. **11**, 15 (2001).
[2] S. Gunes, H. Neugebauer, and N. S. Sariciftci, Chem. Rev. **107**, 1324 (2007).
[3] S. H. Park, A. Roy, S. Beaupre, S. Cho, N. Coates, J. S. Moon, D. Moses, M. Leclerc, K. Lee, and A. J. Heeger, Nat. Photonics **3**, 297 (2009).
[4] H. Y. Chen, J. H. Hou, S. Q. Zhang, Y. Y. Liang, G. W. Yang, Y. Yang, L. P. Yu, Y. Wu, and G. Li, Nat. Photonics **3**, 649 (2009).
[5] P. Peumans, A. Yakimov, and S. R. Forrest, J. Appl. Phys. **93**, 3693 (2003).
[6] H. Hoppe and N. S. Sariciftci, J. Mater. Chem. **16**, 45 (2006).
[7] L. M. Chen, Z. R. Hong, G. Li, and Y. Yang, Adv. Mater. **21**, 1434 (2009).
[8] R. Giridharagopal and D. S. Ginger, J. Phys. Chem. Lett. **1**, 1160 (2010).
[9] C. J. Brabec, M. Heeney, I. McCulloch, and J. Nelson, Chem. Soc. Rev. **40**, 1185 (2011).
[10] T. A. M. Ferenczi, J. Nelson, C. Belton, A. M. Ballantyne, M. Campoy-Quiles, F. M. Braun, and D. D. C. Bradley, J. Phys.-Condens. Mat. **20**, 475203 (2008).
[11] A. L. Ayzner, C. J. Tassone, S. H. Tolbert, and B. J. Schwartz, J. Phys. Chem. C **113**, 20050 (2009).
[12] D. H. Wang, D. G. Choi, K. J. Lee, S. H. Im, O. O. Park, and J. H. Park, Org. Electron. **11**, 1376 (2010).
[13] B. A. Collins, E. Gann, L. Guignard, X. He, C. R. McNeill, and H. Ade, J. Phys. Chem. Lett. **1**, 3160 (2010).
[14] K. H. Lee, P. E. Schwenn, A. R. G. Smith, H. Cavaye, P. E. Shaw, M. James, K. B. Krueger, I. R. Gentle, P. Meredith, and P. L. Burn, Adv. Mater. **23**, 766 (2011).
[15] N. D. Treat, M. A. Brady, G. Smith, M. F. Toney, E. J. Kramer, C. J. Hawker, and M. L. Chabinyc, Advanced Energy Materials **1**, 82 (2011).

[16]J. S. Moon, C. J. Takacs, Y. M. Sun, and A. J. Heeger, Nano. Lett. **11**, 1036 (2011).
[17]W. L. Ma, C. Y. Yang, X. Gong, K. Lee, and A. J. Heeger, Adv. Funct. Mater. **15**, 1617 (2005).
[18]Y. Kim, S. A. Choulis, J. Nelson, D. D. C. Bradley, S. Cook, and J. R. Durrant, Appl. Phys. Lett. **86**, 063502 (2005).
[19]V. D. Mihailetchi, H. X. Xie, B. de Boer, L. J. A. Koster, and P. W. M. Blom, Adv. Funct. Mater. **16**, 699 (2006).
[20]J. G. Labram, E. B. Domingo, N. Stingelin, D. D. C. Bradley, and T. D. Anthopoulos, Adv. Funct. Mater. **21**, 356 (2011).
[21]T. Agostinelli, S. Lilliu, J. G. Labram, M. Campoy-Quiles, M. Hampton, E. Pires, J. Rawle, O. Bikondoa, D. D. C. Bradley, T. D. Anthopoulos, J. Nelson, and J. E. Macdonald, Adv. Funct. Mater. **21**, 1701 (2011).
[22]E. J. Meijer, D. M. de Leeuw, S. Setayesh, E. Van Veenendaal, B. H. Huisman, P. W. M. Blom, J. C. Hummelen, U. Scherf, and T. M. Klapwijk, Nat. Mater. **2**, 678 (2003).
[23]E. C. P. Smits, T. D. Anthopoulos, S. Setayesh, E. Van Veenendaal, R. Coehoorn, P. W. M. Blom, B. de Boer, and D. M. de Leeuw, Phys. Rev. B **73**, 205316 (2006).
[24]P. H. Wobkenberg, D. D. C. Bradley, D. Kronholm, J. C. Hummelen, D. M. de Leeuw, M. Colle, and T. D. Anthopoulos, Synthetic. Met. **158**, 468 (2008).
[25]T. D. Anthopoulos, B. Singh, N. Marjanovic, N. S. Sariciftci, A. M. Ramil, H. Sitter, M. Colle, and D. M. de Leeuw, Appl. Phys. Lett. **89**, 213504 (2006).
[26]J. Zaumseil and H. Sirringhaus, Chem. Rev. **107**, 1296 (2007).
[27]G. Horowitz, J. Mater. Res. **19**, 1946 (2004).
[28]E. Kuwahara, Y. Kubozono, T. Hosokawa, T. Nagano, K. Masunari, and A. Fujiwara, Appl. Phys. Lett. **85**, 4765 (2004).
[29]J. G. Labram, P. H. Wobkenberg, D. D. C. Bradley, and T. D. Anthopoulos, Org. Electron. **11**, 1250 (2010).
[30]A. Dodabalapur, H. E. Katz, L. Torsi, and R. C. Haddon, Science **269**, 1560 (1995).
[31]R. Capelli, S. Toffanin, G. Generali, H. Usta, A. Facchetti, and M. Muccini, Nat. Mater. **9**, 496 (2010).
[32]B. Watts, W. J. Belcher, L. Thomsen, H. Ade, and P. C. Dastoor, Macromolecules **42**, 8392 (2009).
[33]C. Müller, T. A. M. Ferenczi, M. Campoy-Quiles, J. M. Frost, D. D. C. Bradley, P. Smith, N. Stingelin-Stutzmann, and J. Nelson, Adv. Mater. **20**, 3510 (2008).
[34]Y. Kim, S. Cook, S. M. Tuladhar, S. A. Choulis, J. Nelson, J. R. Durrant, D. D. C. Bradley, M. Giles, I. McCulloch, C.-S. Ha, and M. Ree, Nat. Mater. **5**, 197 (2006).
[35]M. C. J. M. Vissenberg and M. Matters, Phys. Rev. B **57**, 12964 (1998).
[36]G. Stephenson, *Mathematical Methods for Science Students* (Pearson, Harlow, 1973), p. 474.
[37]S. Kirkpatrick, Rev. Mod. Phys. **45**, 574 (1973).
[38]R. Fisch and A. B. Harris, Phys. Rev. B **18**, 416 (1978).
[39]H. Kesten, Commun. Math. Phys. **74**, 41 (1980).
[40]D. Chirvase, J. Parisi, J. C. Hummelen, and V. Dyakonov, Nanotechnology **15**, 1317 (2004).